Perovskite Solar Cells

DOI: 10.1002/anie.201406466

A Layered Hybrid Perovskite Solar-Cell Absorber with Enhanced Moisture Stability**

*Ian C. Smith, Eric T. Hoke, Diego Solis-Ibarra, Michael D. McGehee, and Hemamala I. Karunadasa**

Abstract: *Two-dimensional hybrid perovskites are used as absorbers in solar cells. Our first-generation devices containing $(PEA)_2(MA)_2[Pb_3I_{10}]$ (**1**; $PEA = C_6H_5(CH_2)_2NH_3^+$, $MA = CH_3NH_3^+$) show an open-circuit voltage of 1.18 V and a power conversion efficiency of 4.73 %. The layered structure allows for high-quality films to be deposited through spin coating and high-temperature annealing is not required for device fabrication. The 3D perovskite $(MA)[PbI_3]$ (**2**) has recently been identified as a promising absorber for solar cells. However, its instability to moisture requires anhydrous processing and operating conditions. Films of **1** are more moisture resistant than films of **2** and devices containing **1** can be fabricated under ambient humidity levels. The larger bandgap of the 2D structure is also suitable as the higher bandgap absorber in a dual-absorber tandem device. Compared to **2**, the layered perovskite structure may offer greater tunability at the molecular level for material optimization.*

Three-dimensional (3D) hybrid perovskites of the form $(MA)[PbX_3]$ ($MA = CH_3NH_3^+$; X = Cl, Br, or I) have recently emerged as promising absorbers for solar cells.[1] The first reported perovskite solar cell with $(MA)[PbI_3]$ showed a power conversion efficiency (PCE) of 3.81 %.[1a] Rapid material and device optimization has led to PCEs exceeding 15 % in just a few years.[2] Though progress in device efficiencies has been remarkable, the lead–halide perovskites have two main drawbacks: the toxicity of the water-soluble source of lead and the instability of the material to atmospheric moisture. Recently, the lead perovskite was replaced by the significantly less toxic tin analogue in solar cells with efficiencies of up to approximately 6 %.[3] However, the moisture sensitivity of the lead perovskite has not yet been addressed. Motivated by our observations that the structurally related two-dimensional (2D) perovskites readily formed high-quality films that appeared more resistant to humidity than the 3D analogues, we sought to assess if the layered materials could function as solar-cell absorbers. Herein, we report the structure of the layered perovskite $(PEA)_2(MA)_2[Pb_3I_{10}]$ (**1**; $PEA = C_6H_5(CH_2)_2NH_3^+$) that can act as an absorber in a solar cell with an open-circuit voltage of 1.18 V and a PCE of 4.73 %. Although our first-generation devices have lower efficiencies than current solar cells with 3D perovskite absorbers, the layered structure brings distinct advantages. In contrast to $(MA)[PbI_3]$ (**2**), high-quality films of **1** can be obtained through one-step spin coating under ambient conditions without annealing. Films of **1** are also more resistant to moisture compared to **2**, and devices containing **1** can be fabricated under humid conditions. Importantly, the layered structure affords greater tunability, which may provide additional routes for material optimization.

Layered perovskites can be structurally derived from the 3D analogue by slicing along specific crystallographic planes.[4] The interlayer separation and thickness of the inorganic layers can be controlled through the choice of organic cations.[5] The inorganic layers of most layered perovskites comprise a single sheet ($n = 1$) of corner-sharing metal–halide octahedra sandwiching layers of organic cations.[4] These 2D materials do not have electronic properties typically associated with good solar-cell absorbers. Along with larger bandgaps compared to the 3D analogue ($n = \infty$), the spatial confinement of the 2D structure and dielectric mismatch between organic and inorganic layers lead to strongly bound excitons with low mobility.[6] Such tightly bound excitons are difficult to dissociate into free carriers at room temperature and the localized charge carriers are unlikely to reach the electron/hole selective contacts in a typical solar-cell geometry. To access the more favorable electronic properties of the 3D structure, we sought an intermediate structure between the $n = 1$ and $n = \infty$ materials. We synthesized the $n = 3$ member of the series $(PEA)_2(MA)_{n-1}[Pb_nI_{3n+1}]$ (n = number of Pb–I sheets in each inorganic layer), by combining (PEA)I, (MA)I, and PbI_2 in a 2:2:3 stoichiometric ratio in a solvent mixture of nitromethane/acetone. Slow solvent evaporation afforded dark red crystals of $(PEA)_2(MA)_2[Pb_3I_{10}]$ (**1**), the first crystallographically characterized $n = 3$ lead perovskite (Figure 1).

Decreasing the dimensionality of the inorganic components from the 3D structure causes an increase in the bandgap and the exciton binding energy. The reported $n = 1$ and 2 structures have bandgaps of 2.57 and 2.32 eV, respectively, and exciton absorption bands at 2.35 and 2.15 eV, respectively.[7] Their exciton binding energies can be estimated as the difference between bandgap and exciton absorption energies to be 220 and 170 meV for the $n = 1$ and 2 structures,

[*] I. C. Smith, Dr. D. Solis-Ibarra, Prof. H. I. Karunadasa
Department of Chemistry, Stanford University
Stanford, CA 94305 (USA)
E-mail: hemamala@stanford.edu
Dr. E. T. Hoke, Prof. M. D. McGehee
Department of Materials Science and Engineering
Stanford University, Stanford, CA 94305 (USA)

[**] This research was funded by the Global Climate and Energy Project. X-ray diffraction studies were performed at the Stanford Nanocharacterization Laboratory. We thank William Nguyen and Greyson Christoforo for experimental assistance.

Supporting information for this article is available on the WWW under http://dx.doi.org/10.1002/anie.201406466.

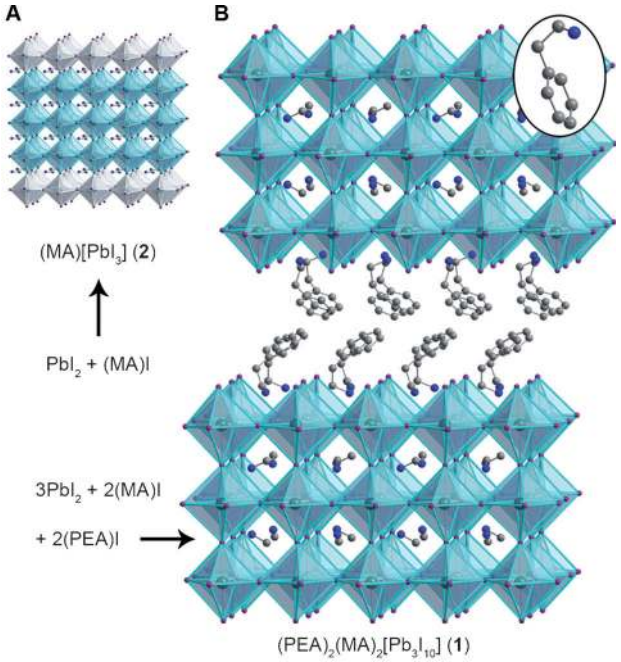

Figure 1. A) Crystal structures of the 3D perovskite (MA)[PbI_3] (**2**, from Ref. [12a]) and B) the 2D perovskite $(PEA)_2(MA)_2[Pb_3I_{10}]$ (**1**). The inorganic layers in **1** can be structurally derived from **2** by slicing along specific crystallographic planes (turquoise sheets in (A)). Inset: a PEA cation in the organic layers. Atom colors: Pb = turquoise; I = purple; N = blue; C = gray. Disordered atoms and hydrogens omitted for clarity.

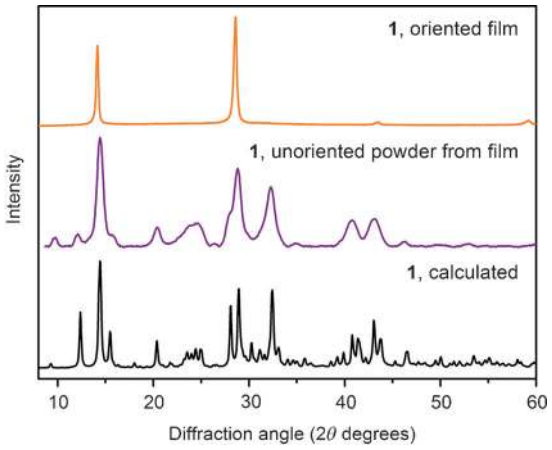

Figure 2. Powder X-ray diffraction (PXRD) patterns of $(PEA)_2(MA)_2[Pb_3I_{10}]$ (**1**) as an oriented film (top) and as powder scraped from a film and measured in a glass capillary (middle), and the calculated PXRD pattern from the single-crystal X-ray structure of **1** (bottom).

respectively.[7] Absorbance measurements of **1** show the exciton band at 2.06 eV, which lies close to an estimated bandgap of approximately 2.1 eV, indicating that the exciton binding energy is significantly smaller and close to the value of **2** (circa 40 meV).[6] The bandgap of **1** is larger than that of **2** (1.61 eV)[8] and larger than the ideal value of 1.34 eV calculated by Shockley and Queisser for the highest efficiency obtainable by a single-junction solar cell (circa 34%).[9] However, **1** can absorb a significant fraction of the solar spectrum to afford a theoretical PCE of approximately 20%. The bandgap of **1** is also close to the ideal value (1.9 eV) for the higher bandgap absorber in a dual-absorber tandem device,[10] which can exceed the Shockley-Queisser limit.[11]

High-quality films of **1** can be deposited from precursor solutions through one-step spin coating. Similar processing of **2** does not afford continuous films (see Figure S1 in the Supporting Information). The layered structure of **1** likely aids film formation: unlike **2** that crystallizes as rhombic dodecahedra at room temperature,[12] **1** forms plates (Figure S2). Powder X-ray diffraction (PXRD) patterns of films of **1** show reflections indicating a preferential orientation of crystallites (Figure 2, top). To confirm the $n = 3$ perovskite structure in these films, we scraped the films into a powder, loaded it into a glass capillary, and obtained unoriented PXRD patterns (Figure 2, middle). These unoriented PXRD data show the reflections calculated from the single-crystal X-ray structure of **1** (Figure 2, bottom). The absorption spectrum of films of **1** shows exciton absorption bands at 2.06, 2.19, and 2.41 eV (Figure S4). We assign the peak at 2.06 eV to the $n = 3$ material. The peaks at 2.19 and 2.41 eV match the exciton absorption energies of the $n = 2$ and $n = 1$ structures, respectively.[5c,13] These phases are not visible in the PXRD patterns of films of **1**, suggesting defect layers of less than $n = 3$ within the structure. Small amounts of $n = 1$ and 2 phases can show in the absorption spectrum because of the high oscillator strength of excitons in these materials.[13] Slight shoulders at 1.94 and 1.87 eV may be caused by trace amounts of $n = 4$ and 5 phases, respectively. The absorption spectrum does not show peaks corresponding to **2** (Figure S4). When excited at 2.54 eV, the emission spectrum of **1** shows a peak at 1.68 eV (Figure S5). This energy lies between the emission maxima for 2D perovskites with lower values of n ($n = 1$ at 2.36 eV[13] and $n = 2$ at 2.15 eV[14]) and the 3D perovskite ($n = \infty$ at 1.58 eV). A weak emission at 2.36 eV is likely because of photoluminescence (PL) from $n = 1$ layers.

Devices utilizing **1** as the absorber were constructed employing TiO_2 as the electron-selective contact and 2,2′,7,7′-tetrakis-(*N*,*N*-di-*p*-methoxyphenylamine)-9,9′-spirobifluorene (spiro-OMeTAD) as the hole-selective contact. Films of **1** were deposited from a *N*,*N*-dimethylformamide solution containing stoichiometric quantities of PbI_2, (MA)I, and (PEA)I using a single spin-coating step. Importantly, devices containing **1** can be processed in humid air, which does not affect film quality or device performance. In contrast, devices with **2** must be processed under low-humidity levels for optimal performance. High-quality films of **2** also require high-temperature thermal evaporation[2b] or multistep deposition methods, such as heat-assisted conversion of spin-coated PbI_2 films to the perovskite through exposure to (MA)I solution[15] or vapor,[2a] or simultaneous deposition of $PbCl_2$ and (MA)I and high-temperature annealing.[16] A scanning electron microscopy (SEM) image of a fully constructed device is shown in Figure 3A. Typical thicknesses of TiO_2, **1**, spiro-OMeTAD, and gold layers are 50, 425, 125, and 75 nm, respectively. We obtained current–voltage (*JV*) curves of these devices using simulated AM1.5G solar illumination (Figure 3B). The open-circuit voltages (V_{oc}) for these devices

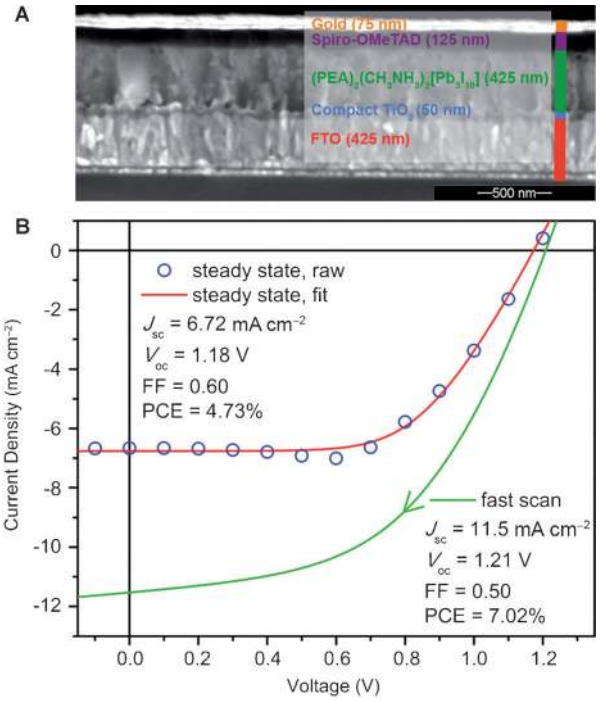

Figure 3. A) SEM cross section and device configuration of planar devices utilizing $(PEA)_2(MA)_2[Pb_3I_{10}]$ (**1**) as the absorber layer. Scale bar = 500 nm. B) Current–voltage (*JV*) curves for the devices fabricated as given in (A).

routinely exceed 1.0 V; the best device shows a value of 1.18 V. Owing to the larger bandgap of the 2D material, these V_{oc} values are higher than for cells containing **2** (highest reported $V_{oc} = 0.924$–1.07 V).[2a–c,15] The increase in V_{oc} value of approximately 0.1 eV correlates well with the measured 0.1 eV increase in the peak PL energy (Figure S5), indicating that carriers are extracted from the same energy levels where radiative recombination occurs.

The *JV* curve characteristics of these devices are sensitive to measurement speed. Faster scan rates afforded a maximum current density of 11.53 mA cm^{-2}, a V_{oc} value of 1.21 V, and a PCE of 7.02%, but the forward and reverse scans showed a large hysteresis (Figure S8). Similar effects have been detected in thin-film devices with **2**.[17] To minimize these effects, the current densities were measured at each voltage after a delay period (70 s) to allow the current to approach steady-state conditions (Figure S9). Even at this slow measurement rate, there is a slight overestimation of photocurrent near the maximum-power point as a result of slow, capacitive effects. We therefore fit the data to the characteristic solar-cell equation (Figure S9) in order to obtain more reliable values of 0.60 for the fill factor (FF) and 4.73% for the PCE. The current density under short-circuit conditions (J_{sc}) is 6.72 mA cm^{-2}. The external quantum efficiency (EQE) spectrum matches the profile of the absorption spectrum of **1** (Figure S10). The integrated current from the EQE spectrum yields a net current density of 7.47 mA cm^{-2}, corroborating the J_{sc} value obtained through steady-state measurements. We calculate an internal quantum efficiency of 70%, assuming 10% parasitic absorbance by non-absorber components of the device. This indicates that charge extraction could be limited, caused likely by the layered structure of **1**, which has no direct path between adjacent inorganic layers. Low-dimensional inorganic materials have previously been effectively used in photovoltaic devices,[18] and device optimization should afford improvements in J_{sc} values and overall efficiency.

Upon exposure to ambient humidity at room temperature, opaque black films of **2** convert into a translucent yellow solid.[12b,19] Finished devices containing **2** can be encapsulated to avoid exposure to water. However, inherent stability to moisture will likely be necessary for large-scale manufacture or for achieving the long lifetimes required for broad commercialization. To compare the stability of **1** and **2** to moisture, we exposed spin-coated films of both materials to humidity-controlled environments. Because direct spin coating results in poor-quality, discontinuous films of **2** (denoted **2a**), we also formed higher-quality films of $(MA)[PbI_3]$ (denoted **2b**) by depositing a 1:3 molar ratio of $PbCl_2$:(MA)I and annealing the films at 100 °C.[16] All films were exposed to a relative humidity level of 52% for up to approximately 40 days and their PXRD patterns were periodically recorded (Figure 4). Upon humidity exposure, the PXRD patterns of

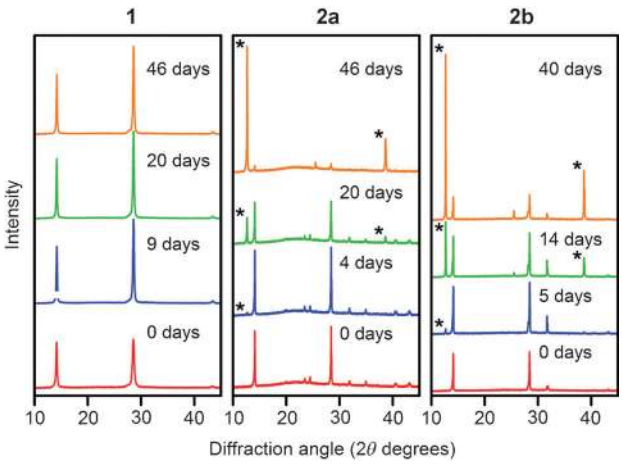

Figure 4. PXRD patterns of films of $(PEA)_2(MA)_2[Pb_3I_{10}]$ (**1**), $(MA)[PbI_3]$ formed from PbI_2 (**2a**), and $(MA)[PbI_3]$ formed from $PbCl_2$ (**2b**), which were exposed to 52% relative humidity. Annealing of films of **2a** (15 minutes) and **2b** (80 minutes) was conducted at 100 °C prior to humidity exposure. Asterisks denote the major reflections from PbI_2.

2a and **2b** show a new phase after circa 4–5 days, which can be indexed to the PXRD pattern of PbI_2 (Figure S11). These new reflections completely dominate the PXRD patterns after approximately 40 days. Absorption spectra of **2a** and **2b** show a decrease in absorbance near the bandgap and an increase in absorbance above 2.4 eV (Figures S12 and 13) as the higher-bandgap PbI_2 phase grows as yellow patches on the films (Figure S14). In contrast, the PXRD pattern of **1** does not show additional reflections over a period of 46 days of humidity exposure and the absorption spectra show no significant changes over this time (Figure S15).

We show that a layered Pb–I perovskite can act as a solar-cell absorber. The $n = 3$ perovskite takes an intermediate

position between $n=1$ perovskites with strongly bound excitons and $n=\infty$ perovskites with weakly bound excitons. Strongly bound excitons in $n=1$ Pb–I perovskites lead to green PL,[20] and green electroluminescence,[14,21] and we recently reported on broadband white PL from Pb–Br perovskites.[22] In contrast, weakly bound excitons and shallow trap states could contribute to the unusually long carrier diffusion lengths seen in $n=\infty$ perovskites.[23] These dramatic changes in electronic properties as a function of the structural evolution from $n=1$ to $n=\infty$ are of both fundamental and technological interest.

Solar cells containing **1** display PCEs up to 4.73%. Though devices containing **2** have exceeded PCEs of 15%,[2a–c] their moisture sensitivity remains a concern for large-scale device fabrication or their long-term use. The layered structure of **1** aids the formation of high-quality films that show greater moisture resistance compared to **2**. The larger bandgap of **1** also affords a higher V_{OC} value of 1.18 V compared to devices with **2**. Further improvements in material structure and device engineering, including making appropriate electronic contact with the anisotropic inorganic sheets, should increase the PCEs of these devices. In particular, higher values of n as single-phase materials or as mixtures may allow for lower bandgaps and higher carrier mobility in the inorganic layers while the organic layers provide additional tunability. For example, hydrophobic fluorocarbons could increase moisture stability, conjugated organic layers could facilitate charge transport, and organic photosensitizers could improve the absorption properties of the material. We are focused on manipulating this extraordinarily versatile platform through synthetic design.

Received: June 22, 2014
Revised: July 30, 2014
Published online: ■■ ■■, ■■■■

Keywords: layered compounds · materials science · perovskite · photovoltaics · solar cells

[1] a) A. Kojima, K. Teshima, Y. Shirai, T. Miyasaka, *J. Am. Chem. Soc.* **2009**, *131*, 6050 – 6051; b) J.-H. Im, C.-R. Lee, J.-W. Lee, S.-W. Park, N.-G. Park, *Nanoscale* **2011**, *3*, 4088 – 4093; c) M. M. Lee, J. Teuscher, T. Miyasaka, T. N. Murakami, H. J. Snaith, *Science* **2012**, *338*, 643 – 647; d) L. Etgar, P. Gao, Z. Xue, Q. Peng, A. K. Chandiran, B. Liu, M. K. Nazeeruddin, M. Grätzel, *J. Am. Chem. Soc.* **2012**, *134*, 17396 – 17399.

[2] a) J. Burschka, N. Pellet, S.-J. Moon, R. Humphry-Baker, P. Gao, M. K. Nazeeruddin, M. Grätzel, *Nature* **2013**, *499*, 316 – 319; b) M. Liu, M. B. Johnston, H. J. Snaith, *Nature* **2013**, *501*, 395 – 398; c) D. Liu, T. L. Kelly, *Nat. Photonics* **2014**, *8*, 133 – 138; d) S. Kazim, M. K. Nazeeruddin, M. Grätzel, S. Ahmad, *Angew. Chem. Int. Ed.* **2014**, *53*, 2812 – 2824; *Angew. Chem.* **2014**, *126*, 2854 – 2867.

[3] a) F. Hao, C. C. Stoumpos, D. H. Cao, R. P. H. Chang, M. G. Kanatzidis, *Nat. Photonics* **2014**, *8*, 489 – 494; b) N. K. Noel, et al., *Energy Environ. Sci.* **2014**, *7*, 3061 – 3068.

[4] a) D. B. Mitzi, *Prog. Inorg. Chem.* **1999**, *48*, 1 – 121; b) D. B. Mitzi, *J. Chem. Soc. Dalton Trans.* **2001**, 1 – 12.

[5] a) D. B. Mitzi, C. A. Feild, W. T. A. Harrison, A. M. Guloy, *Nature* **1994**, *369*, 467 – 469; b) D. B. Mitzi, S. Wang, C. A. Feild, C. A. Chess, A. M. Guloy, *Science* **1995**, *267*, 1473 – 1476; c) J. Calabrese, N. L. Jones, R. L. Harlow, N. Herron, D. L. Thorn, Y. Wang, *J. Am. Chem. Soc.* **1991**, *113*, 2328 – 2330.

[6] E. A. Muljarov, S. G. Tikhodeev, N. A. Gippius, T. Ishihara, *Phys. Rev. B* **1995**, *51*, 14370 – 14378.

[7] T. Ishihara, *J. Lumin.* **1994**, *60 – 61*, 269 – 274.

[8] Y. Yasuhiro, N. Toru, E. Masaru, W. Atsushi, K. Yoshihiko, *Appl. Phys. Express* **2014**, *7*, 032302.

[9] W. Shockley, H. J. Queisser, *J. Appl. Phys.* **1961**, *32*, 510 – 519.

[10] A. D. Vos, *J. Phys. D* **1980**, *13*, 839 – 846.

[11] a) A. S. Brown, M. A. Green, *Physica E* **2002**, *14*, 96 – 100; b) Z. M. Beiley, M. D. McGehee, *Energy Environ. Sci.* **2012**, *5*, 9173 – 9179.

[12] a) C. C. Stoumpos, C. D. Malliakas, M. G. Kanatzidis, *Inorg. Chem.* **2013**, *52*, 9019 – 9038; b) T. Baikie, Y. Fang, J. M. Kadro, M. Schreyer, F. Wei, S. G. Mhaisalkar, M. Graetzel, T. J. White, *J. Mater. Chem. A* **2013**, *1*, 5628 – 5641.

[13] X. Hong, T. Ishihara, A. V. Nurmikko, *Phys. Rev. B* **1992**, *45*, 6961 – 6964.

[14] X. Hong, T. Ishihara, A. V. Nurmikko, *Solid State Commun.* **1992**, *84*, 657 – 661.

[15] Q. Chen, H. Zhou, Z. Hong, S. Luo, H.-S. Duan, H.-H. Wang, Y. Liu, G. Li, Y. Yang, *J. Am. Chem. Soc.* **2014**, *136*, 622 – 625.

[16] G. E. Eperon, V. M. Burlakov, P. Docampo, A. Goriely, H. J. Snaith, *Adv. Funct. Mater.* **2014**, *24*, 151 – 157.

[17] H. J. Snaith, et al., *J. Phys. Chem. Lett.* **2014**, *5*, 1511 – 1515.

[18] a) T. T. Ngo, S. Chavhan, I. Kosta, O. Miguel, H.-J. Grande, R. Tena-Zaera, *ACS Appl. Mater. Interfaces* **2014**, *6*, 2836 – 2841; b) M. Calixto-Rodriguez, H. M. García, M. T. S. Nair, P. K. Nair, *ECS J. Solid State Sci. Technol.* **2013**, *2*, Q69 – Q73.

[19] J. H. Noh, S. H. Im, J. H. Heo, T. N. Mandal, S. I. Seok, *Nano Lett.* **2013**, *13*, 1764 – 1769.

[20] K. Gauthron, et al., *Opt. Express* **2010**, *18*, 5912 – 5919.

[21] a) M. Era, S. Morimoto, T. Tsutsui, S. Saito, *Appl. Phys. Lett.* **1994**, *65*, 676 – 678; b) K. Chondroudis, D. B. Mitzi, *Chem. Mater.* **1999**, *11*, 3028 – 3030.

[22] E. R. Dohner, E. T. Hoke, H. I. Karunadasa, *J. Am. Chem. Soc.* **2014**, *136*, 1718 – 1721.

[23] a) G. Xing, N. Mathews, S. Sun, S. S. Lim, Y. M. Lam, M. Grätzel, S. Mhaisalkar, T. C. Sum, *Science* **2013**, *342*, 344 – 347; b) S. D. Stranks, G. E. Eperon, G. Grancini, C. Menelaou, M. J. P. Alcocer, T. Leijtens, L. M. Herz, A. Petrozza, H. J. Snaith, *Science* **2013**, *342*, 341 – 344.

